Carboxysome-inspired electrocatalysis using enzymes for the reduction of CO_2 at low concentrations

Samuel J. Cobb[1†], Azim M. Dharani[1†], Ana Rita Oliveira[2], Inês A. C. Pereira[2], and Erwin Reisner[1*]

[1]Yusuf Hamied Department of Chemistry, University of Cambridge, Cambridge, U.K

[2] Instituto de Tecnologia Química e Biológica António Xavier (ITQB NOVA), Universidade NOVA de Lisboa, Oeiras, Portugal.

†These authors contributed equally to this work

*Corresponding author. Email: reisner@ch.cam.ac.uk

Abstract

The electrolysis of dilute CO_2 streams suffers from low concentrations of dissolved substrate and its rapid depletion at the electrolyte-electrocatalyst interface. These limitations require first energy-intensive CO_2 capture and concentration, before electrolyzers can achieve acceptable performances. For direct electrocatalytic CO_2 reduction from low-concentration sources, we introduce a strategy that mimics the carboxysome in cyanobacteria by utilizing microcompartments with nanoconfined and concentrated enzymes in a porous electrode. A carbonic anhydrase accelerates CO_2 hydration kinetics and minimizes substrate depletion by making all dissolved carbon available for utilization, while a highly efficient formate dehydrogenase reduces CO_2 cleanly to formate; down to even atmospheric concentrations of CO_2. This bio-inspired concept demonstrates that the carboxysome provides a viable blueprint and strategy to achieve the reduction of low-concentration CO_2 streams to chemicals.

Introduction

As atmospheric CO_2 levels continue to rise and emerging geopolitical issues threaten global energy supplies, novel methods of forming fuels sustainably and without geographic restrictions are required for a secure energy supply in a future net zero carbon economy. The utilization of low concentrations of CO_2 holds considerable promise given its potential to both produce renewable fuels and prevent the release of CO_2 into the atmosphere through the conversion of flue gases, or even directly remove excess CO_2 from the atmosphere.[1] However, electrochemical CO_2 reduction (CO_2R) has so far focused on the utilization of saturated (100%) CO_2 streams as state-of-the-art catalysts perform poorly under low CO_2 concentrations due to the low availability of dissolved CO_2 (12 μM at atmospheric CO_2 concentrations, 420 ppm). As most synthetic CO_2R catalysts exhibit first order kinetics, their activity decreases proportionally with CO_2 concentration, meaning their activity is significantly reduced even at flue gas concentrations. Synthetic catalysts also commonly suffer from side-reactions (in particular hydrogen evolution) that are only marginally affected by CO_2 concentration, thereby decreasing the proportion of energy going towards forming the desired carbon products (*i.e.*, the faradaic efficiency, FE) when utilizing CO_2 from low concentration sources.[2]

While there have been some reports of direct CO_2 reduction at concentrations down to 1%, the low affinity of these systems limit their applicability for atmospheric CO_2 and are often accompanied by the production of significant side products.[2,3] The limitations of current CO_2R systems therefore require emerging carbon capture technologies[4–7] to produce concentrated CO_2 gas streams in order to achieve acceptable performances. However, CO_2 concentration from atmosphere for this stepwise process must incur substantial energy and cost penalties (projected to be 9 GJ ton^{-1} and \$94–232 ton^{-1})[4] to enable efficient carbon capture and utilization from dilute gas streams. This must also be addressed alongside common challenges in capture streams with impurities such as O_2, NO_x and SO_x.[8,9]

Nature does not require such compromises and has evolved efficient approaches to utilize atmospheric CO_2 directly to make complex products (e.g. sugars) using the carboxysome — a membraneless organelle used to efficiently fix CO_2 within cyanobacteria.[10–12] The rate limiting step for cyanobacterial carbon fixation is catalyzed by ribulose-1,5-bisphosphate carboxylase/oxygenase (RuBisCO), which displays a low catalytic rate under reduced CO_2 conditions and competing utilization of O_2.[13,14] The carboxysome provides a microenvironment that overcomes the limitations of RuBisCO by recruiting carbonic anhydrase (CA) and encapsulating both enzymes within the organelle's protein shell (Figure 1a). CA catalyzes the conversion of HCO_3^- to CO_2 within the carboxysome, accelerating the kinetically slow interconversion of HCO_3^- and CO_2 (eq. 1) from an uncatalyzed rate of 0.05 s^{-1} to rates up to $1 \cdot 10^6$ s^{-1}.[15] The fast interconversion of HCO_3^- and CO_2 provides a higher effective concentration of carbon for fixation as all dissolved inorganic carbon species can now be utilized to overcome the concentration limits imposed by using CO_2 alone as the carbon source for RuBisCO.

$$CO_2 + H_2O \overset{CA}{\rightleftharpoons} H_2CO_3 \rightleftharpoons H^+ + HCO_3^- \rightleftharpoons 2H^+ + CO_3^{2-} \quad (\text{eq. } 1)$$

Cyanobacteria further exploit the accelerated interconversion between HCO_3^- and CO_2 for utilization by using HCO_3^- pumps and maintaining an alkaline cytosolic pH. With these strategies, cyanobacteria accumulate high levels of intracellular HCO_3^-, which can be converted to CO_2 by CA to replenish substrate depletion in the carboxysome.[16,17] Together, the nanoconfinement of RuBisCO, enzymatic acceleration of CO_2 hydration kinetics, and accumulation of high HCO_3^- levels enable cyanobacteria to efficiently concentrate and utilize atmospheric CO_2 within carboxysomes.

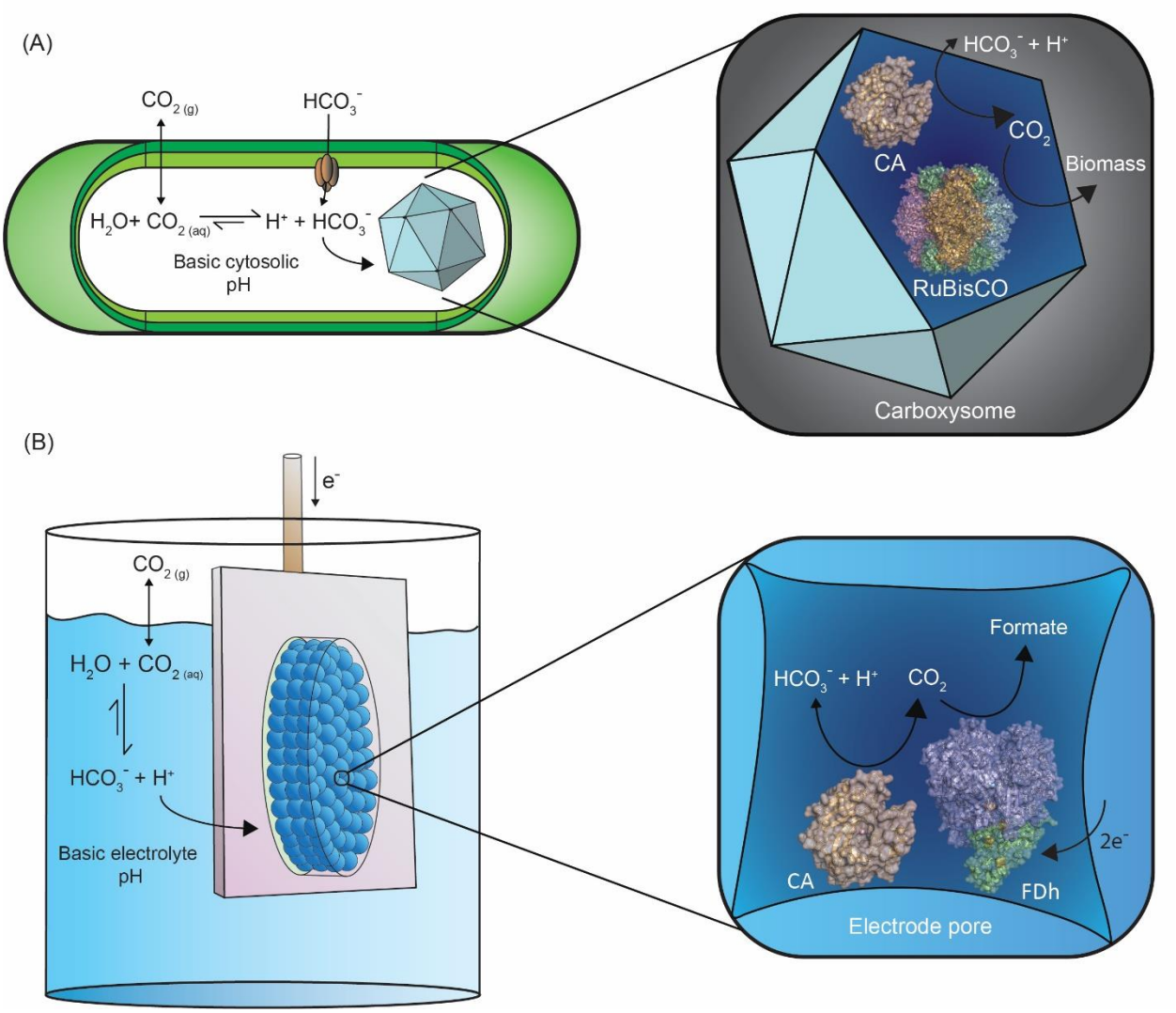

Figure 1. Comparison between cyanobacterial carboxysome and designed bioelectrocatalytic system. (A) Cyanobacteria enhance atmospheric carbon fixation by accumulating high levels of intracellular HCO_3^- through active transport and their basic cytosolic pH. As HCO_3^- diffuses into the nanoconfined carboxysome, CA rapidly dehydrates HCO_3^- to CO_2 to raise local substrate levels for RuBisCO, which serves as the inspiration for co-localizing CA and FDh within the pores of mesoporous electrodes (B) in basic solutions for improved electrocatalytic fuel production under atmospheric conditions.

Similar to its role in cyanobacterial carbon fixation, HCO_3^- offers an energy efficient method for CO_2 concentration,[18] which has been exploited for carbon capture in KOH solutions[4] and has led to the development of bicarbonate[19–22] and carbonate[23] driven electrolyzers. These

HCO_3^- based carbon capture technologies avoid the energy penalties of CO_2 desorption and separation by directly producing products from HCO_3^-. CO_2 capture as HCO_3^- is a conceptually simpler approach than CO_2 capture in amine solutions as carbamates where the CO_2 can be released or reduced directly to form products[24–26], although this suffers from significant drawbacks in terms of energy efficiency and selectivity.

Along with their use in biological systems, enzymes are being explored in electrochemical CO_2R primarily due to their high energy efficiency (low overpotential) and catalytic rates. Enzymes also approach a selectivity of 100% and display a high affinity for CO_2 due to Michaelis-Menten kinetics. These properties offer potentially significant advantages but have not yet been explored for the utilization of low CO_2 concentrations. The fuel-forming enzyme formate dehydrogenase (FDh) has previously been combined with CA for enzymatic CO_2R to demonstrate that CO_2 (and not HCO_3^-) is the substrate of FDh.[27] In addition, CA has been used to catalyze the conversion of CO_2 to HCO_3^-, decreasing local CO_2 concentrations and increasing HCO_3^- and H^+ (directly contrasting its role in increasing CO_2 concentrations in the carboxysome) either to mitigate local pH changes in saturated CO_2[28] or for the use of HCO_3^- as a substrate.[29]

Enzymatic CO_2R at low CO_2 concentrations with CA has also relied on an energy inefficient NADH cofactor recycling system to transfer electrons from an electrode to enzymes in bulk solution giving a low FE and offering no capability to mimic the nanoconfined environment of a carboxysome on an electrode[29–31], a property that may be highly beneficial for CO_2R at reduced rates as it has been shown to improve enzyme's affinity for substrate and kinetic rates.[32] CA has also been used in carbon capture systems[33] to increase the kinetics of CO_2 capture as HCO_3^- and release of carbon capture, but the Faradaic Efficiency (FE) has been significantly reduced when this capture media has been used for electrolysis.[34]

While most carbon capture has focused on producing concentrated CO_2 gas streams or concentrated capture media,[35,36] the integration of capture and utilization into a single system that uses low concentrations of CO_2, ideally down to atmospheric concentrations, offers the potential to minimize the energy and complexity requirements of this process in the manner of the biological carboxysome. In this work, we adapt strategies employed by carboxysomes to enhance direct CO_2R from low-concentration sources by increasing local CO_2 concentrations (flue gas to atmospheric concentrations, 10% – 420 ppm in N_2). CO_2R is performed under nanoconfinement within mesoporous indium tin oxide (ITO) electrodes (SI Figure S1 and S2) to manage the concentration of compartmentalized CO_2, HCO_3^-, and H^+, which are crucial to CO_2R performance. Within the porous electrode, CA accelerates the kinetically slow interconversion between HCO_3^- and CO_2, allowing for the utilization of the total dissolved carbon pool to offset local CO_2 depletion (Figure 1b). The buffer capacity and pH of electrolytes used in this work are altered to raise local HCO_3^- concentrations, which can be converted to CO_2 by CA to mitigate local substrate consumption. With these interventions we raise local CO_2 levels within the nanoconfined electrode, offsetting diffusion gradients and substrate depletion that primarily limit enzymatic fuel production from dilute gas streams. Through these methods we have demonstrated a nanoconfined carboxysome-inspired system for the reduction of low concentrations CO_2 streams, down to atmospheric levels, to formate. This produces quantifiable product concentrations and is underpinned by the use of finite element modelling to provide an understanding of how solution concentrations for all carbon components can be optimized for effective system performance.

Results and Discussion

The tungsten formate dehydrogenase (FDh) from *Desulfovibrio vulgaris* Hildenborough was chosen as the CO_2 reductase for its quantitative selectivity, electrochemical reversibility, non-linear substrate dependence, and high affinity for CO_2 (K_M: 0.42 mM), which makes this FDh ideally suited for the direct utilization of low concentration CO_2 streams (SI Figure S3).[37] FDh can also be co-immobilized with or without CA on mesoporous ITO electrodes (40 nm particle size, 8.5 μm thickness, and 0.19 cm^2 geometric surface area) at lower fuel forming enzyme concentrations than in the natural carboxysome (Table S1, 9.52 mM vs 0.63 mM, 40 pmol total concentration immobilized in the porous electrode) due to FDh's higher activity, with the non-redox active enzyme CA (40 pmol) at comparable concentrations to the carboxysome, catalyzing CO_2 hydration kinetics within the porous electrode. The CO_2 purged aqueous solutions used in this study have a total dissolved carbon concentration that is greater than that of CO_2 alone due to its equilibration to form HCO_3^- and CO_3^{2-} (eq 1), species that cannot directly be utilized as substrates for FDh.[27] Given its commercial availability and fast kinetics, CA from bovine erythrocytes was chosen to accelerate HCO_3^- dehydration, allowing for the utilization of the total inorganic carbon pool to offset CO_2 depletion within the porous electrode. Enzyme electrochemistry experiments informed the development of finite element models (FEM), which demonstrate how experimentally inaccessible components of the local electrochemical environment (compartmentalized CO_2, HCO_3^-, and H^+ concentrations) change with applied potential and electrolyte composition to improve formate production under reduced CO_2 conditions.

Bicarbonate as a semi-artificial carboxysome electrolyte

When the only buffer system in the electrolyte was CO_2 and its conjugate base HCO_3^-, which is inherently present when CO_2 is purged into solution at neutral pH (eq. 1), CA co-immobilization at concentrations comparable to the natural carboxysome (~mM, 40 pmol loaded, Table S1) had no significant effect on the enzymatic CO_2R rate with negligible difference in reduction cur-

rent densities from cyclic voltammetry (Figure S4a). Constant potential electrolysis was performed in triplicate for product quantification at each applied potential and formate quantified using ion chromatography to calculate FEs and average partial current densities (Figure 2a). The formate partial current density of CO_2R by immobilized FDh ($j_{formate}$, points, Figure 2a) in 1% and 10% CO_2 purged solutions with N_2 as the balance gas, unlike when purged with concentrated CO_2[28], was not affected by CA co-immobilization. Formate was the quantitative product as no other liquid or gas phase products (such as H_2, CO or CH_4) were detected by ion chromatography or headspace gas chromatography, respectively (for total and partial current densities from all experiments including controls see Table S2). At 10% CO_2, the co-immobilization of CA increased the $j_{formate}$ from −63 ± 17 μA cm^{-2} to −72 ± 37 μA cm^{-2} and at 1% the co-immobilization of CA decreased the $j_{formate}$ from −10 ± 4 μA cm^{-2} to −8 ± 4 μA cm^{-2} at −0.6 V vs SHE. The FE for $HCOO^-$ at –0.6 V vs SHE was 83 ± 8% at 10% CO_2 and 54 ± 7% at 1% CO_2.

While we have previously shown that FDh produces formate with nearly 100% FE under pure CO_2 on ITO,[28,38] the reduced FE under low CO_2 concentrations can be tentatively attributed to the residual background reduction of the metal oxide electrode.[39–41] This can be observed in the absence of enzymes with no liquid or gaseous products being detected by Ion or Gas Chromatography, respectively (Figure S5) at current densities that match well with the unattributed FE under low CO_2 concentrations. As the reduction products of ITO cannot be quantified by liquid or gas phase techniques during electrolysis with enzymes a FE is not reported for this reaction. However, in the absence of any other detected solution or gas phase products it is expected that ITO reduction, which has a current density that is invariant on CO_2 concentration, is a significant contribution to the remaining FE and is consistent with the trend for decreased formate FE with reduced total current densities.

A Finite Element Model (FEM) using a previously reported approach[28,38] was used to model the local environment that was experimentally inaccessible (Figure S6).[42] This uses well

understood physical and analytical equations, with enzyme properties determined from solution assays,[37] solved over a mesh that represents the geometry of the system to model the response and was in good agreement with experimentally observed currents (lines, Figure 2a), allowing the concentrations of species within the porous electrode to be determined (Figure 2b–c).

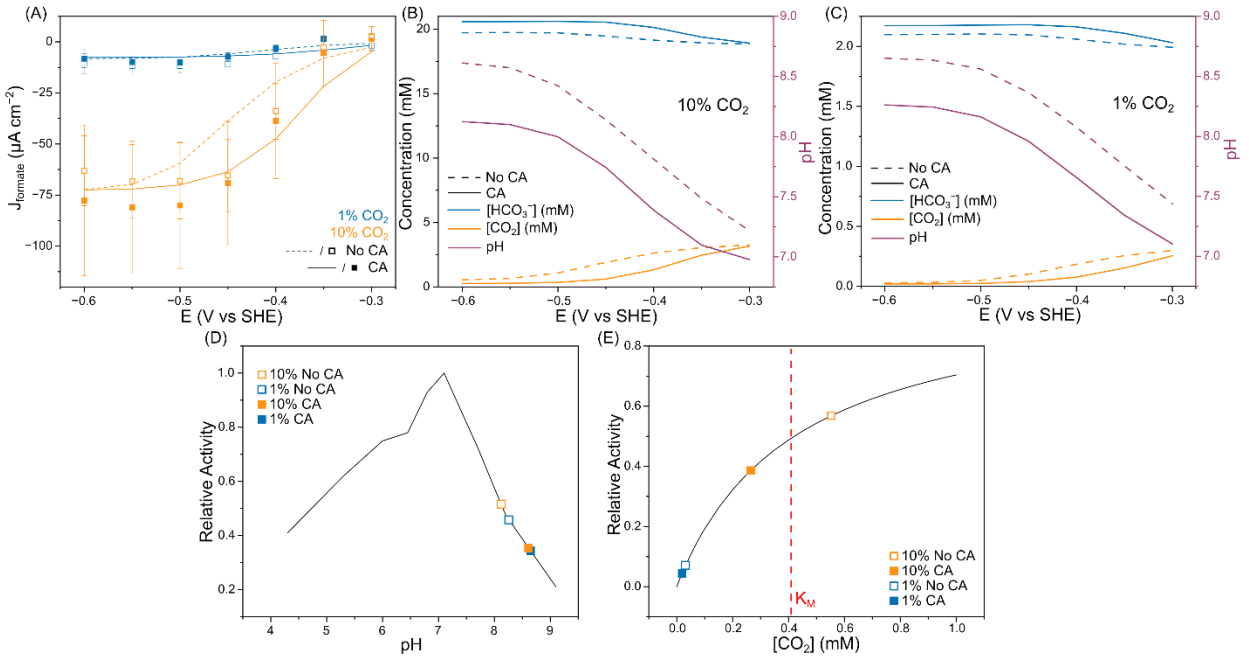

Figure 2. The electrochemical performance and simulated local environment of FDh (40 pmol) with and without CA (40 pmol) co-immobilization in $NaHCO_3$ containing solutions at 10 and 1% CO_2. (A) Experimental and simulated partial formate current densities from constant potential electrolysis between −0.3 and −0.6 V vs SHE for $NaHCO_3$ purged with 1% (blue) and 10% (orange) CO_2 at pH 7. (B+C) Volume average local concentrations of CO_2 (orange), HCO_3^- (blue) and pH (purple, right y axis) within the porous electrode domain from FEM at all tested overpotentials in 10% (B) and 1% (C) purged solutions. Local pH (D) and CO_2 (E) obtained from FEM at the highest tested overpotentials and their relative impacts on the pH (D) and CO_2 concentration (E) dependent activity of FDh for CO_2R determined from solution assays.[37] Solution conditions: $NaHCO_3$ containing 50 mM KCl purged with 1 or 10% CO_2 and adjusted to pH 7.0 with

$NaHCO_3$ after gas equilibration. Solid and hollow squares represent conditions with and without CA respectively.

It is apparent that the comparable currents with and without accelerated CO_2 hydration kinetics are due to very different local environments at both 10 (Figure 2b) and 1% CO_2 (Figure 2c). In both cases the local pH and [CO_2] are reduced, and the [HCO_3^-] is increased when CA is co-immobilized. These changes can be attributed to the accelerated conversion of CO_2 and H_2O to HCO_3^- and H^+ promoted to mitigate the local pH increase within the mesoporous electrode. The basic local environment results from the catalyst depleting CO_2 and H^+ within the electrode to produce formic acid which dissociates to $HCOO^-$ and H^+, consuming 1 net proton (eq. 2).

$$CO_2 + 2H^+ + 2e^- \xrightarrow{FDh} HCOO^- + H^+ \quad (eq.\ 2)$$

Without CA, the interconversion of CO_2 and HCO_3^- is slow, and the depleted CO_2 and H^+ are predominantly replenished by diffusion from the bulk solution, as opposed to the equilibration of CO_2 with HCO_3^-. When CA is present, the rate of CO_2 and HCO_3^- interconversion is increased, allowing the CO_2 and HCO_3^- concentrations to follow the chemical equilibria in solution. The more basic pH formed within the electrode favors the conversion of CO_2 to H^+ and HCO_3^-, in competition with the depletion of CO_2 favoring the reverse reaction. In both 10% and 1% CO_2 purged solutions (bulk [CO_2] = 3.2 and 0.32 mM, respectively), local CO_2 concentrations are further depleted with fast CO_2 hydration kinetics (0.55 vs 0.26 mM at −0.6 V vs SHE with 10% CO_2 and 28 vs 19 μM at −0.6 V vs SHE with 1% CO_2), due to the conversion of CO_2 into HCO_3^- and H^+ to mitigate the local pH change. This leads to a lower local pH at all CO_2 concentrations (8.61 vs 8.12 pH and 8.65 vs 8.26 at −0.6 V vs SHE for 10% CO_2 and 1% CO_2, respectively), at the expense of CO_2 concentration when CA is introduced.

Although the decreased local pH marginally increases FDh activity (Figure 2d), the additional consumption of CO_2 required to mitigate the local pH change decreases enzymatic CO_2R (Figure 2e). These effects on enzyme activity counteract one another and are responsible for the lack of improved rates of fuel production with increased CO_2 hydration kinetics. FEM explains why CA does not improve formate production in these solutions as CO_2 acts as both the substrate and primary buffer, highlighting the trade-off in maintaining an optimal local pH and high substrate levels under reduced CO_2 concentrations.

Maintaining local CO_2 concentrations using Good's buffers for pH regulation

Under all conditions, the addition of the kinetically fast Good's buffer 3-(N-morpholino)propane sulfonic acid (MOPS) substantially improves the CO_2R current density. This buffer system was chosen because the pK_a of MOPS is close to the optimal pH for FDh (7.1), and the electrolyte does not affect the FDh activity.[38] CA co-immobilization significantly increased the observed $j_{formate}$ 1.7× from −135 ± 26 to −235 ± 37 μA cm^{-2} in 10% CO_2 purged pH 7 MOPS solutions at −0.6 V vs SHE (Figure 3a), with a FE of 91 ± 5 and 96±6 % from 2 h experiments to produce sufficient product for quantification in the presence and absence of CA co-immobilization respectively. Exemplar CVs are also shown in Figure S4b. In 1% CO_2 purged pH 7 MOPS solutions, a larger increase in $j_{formate}$ of 3.1× from −16.3 ± 0.35 to −51 ± 7 μA cm^{-2} was observed upon CA co-immobilization, with FEs of 63 ± 2 and 74 ±5 % in the absence and presence of CA co-immobilization, respectively.

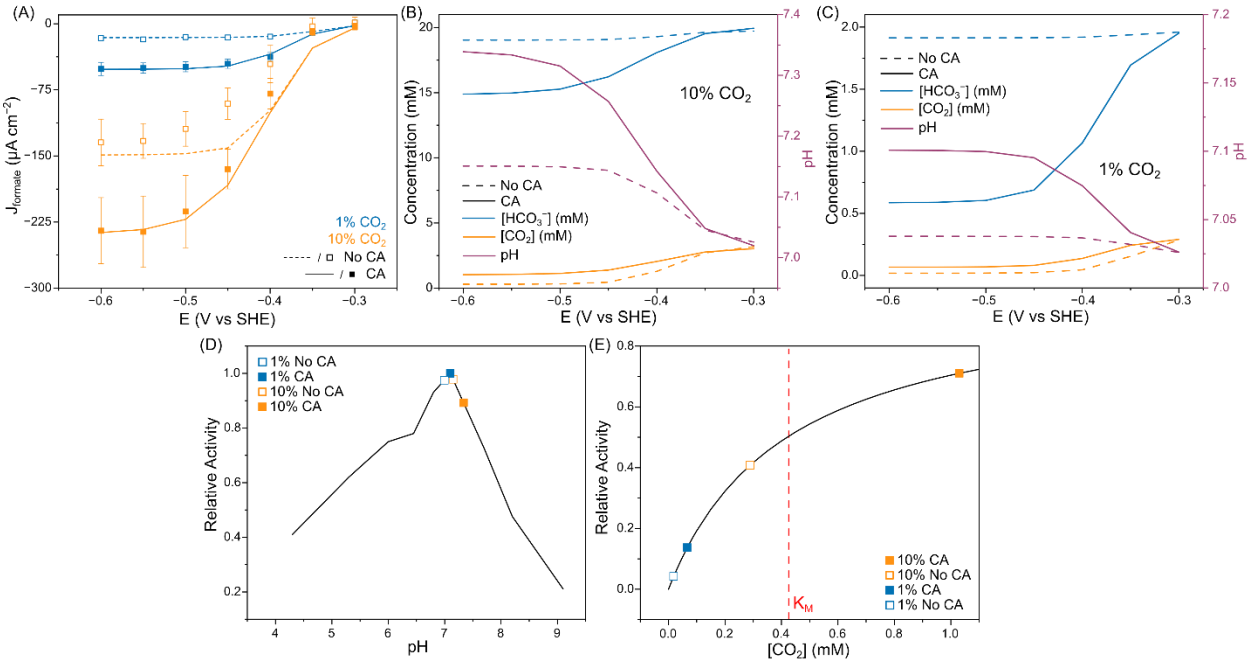

Figure 3. The electrochemical performance and simulated local environment of FDh (40 pmol) with and without CA (40 pmol) co-immobilization in 0.1 M MOPS solutions at 10 and 1% CO_2. (**A**) Experimental and simulated current densities from constant potential electrolysis between −0.3 and −0.6 V vs SHE for 0.1 M MOPS purged with 1% (blue) and 10% (orange) CO_2 at pH 7. (B and C**)** Local concentrations of CO_2 (orange), HCO_3^- (blue) and pH (purple, right y axis) within the porous electrode from FEM at all tested overpotentials in 10% (B) and 1% (C) purged solutions. Local pH (D) and CO_2 (E) obtained from FEM at the highest tested overpotentials and their relative impacts on enzymatic CO_2R. Solution conditions: 0.1 M MOPS containing 50 mM KCl purged with 1 or 10% CO_2 and adjusted to pH 7.0 with $NaHCO_3$ after gas equilibration. Solid and hollow squares represent conditions with and without CA respectively.

In the absence of CA, the addition of MOPS reduces the pH increase within the electrode compared to $NaHCO_3$ (pH 8.61 vs 7.15 and pH 8.65 vs 7.03 at −0.6 V vs SHE, bulk pH= 7.0). A slightly increased local pH was witnessed in the FEM when CA was immobilized (7.34 vs 7.15 and 7.10 vs 7.03 for 10 and 1% CO_2 purged MOPS, respectively (Figure 3b–c)). The depletion of CO_2 within the porous electrode dominates the observed electrochemical response (Figure 3d) and the minimal increase in local pH has little effect on the enzyme activity (Figure 3e). The addition of CA promotes the conversion of HCO_3^- and H^+ into CO_2 to offset local substrate consumption in MOPS containing solutions, increasing the local [CO_2], reducing the

[HCO_3^-] with only a small increase in the local pH (Figure 3b–c). This contrasts the activity of CA observed in solutions without MOPS in which the large local pH increase promoted the reverse reaction to liberate H^+ and consume CO_2 to resist the pH change. The co-immobilization of CA results in significantly elevated local CO_2 concentrations (1.03 vs 0.29 mM and 66 µM vs 18 µM at −0.6 V vs SHE for 10% and 1% bulk CO_2, respectively (Figure 3e)), causing a large improvement in the rate of enzymatic CO_2R.

While the relative increase in local CO_2 concentration is similar when CA is introduced at 10 and 1% CO_2, the improvement in CO_2R current density is greater at 1% CO_2 since the rate of fuel production becomes more dependent on available substrate concentrations as purged CO_2 levels decrease below the K_M of FDh towards atmospheric concentrations. Much like the co-localization of CA and RuBisCO within carboxysomes, fast CO_2 hydration kinetics improve enzymatic CO_2R within the nanoconfined mesoporous electrode by increasing available CO_2 concentrations through the utilization of HCO_3^- as an indirect carbon source in well buffered solutions that remove the requirement of the carbon pool to act as a buffer system.

Increasing pH to increase local total carbon concentrations

As CA consumes HCO_3^- to increase local CO_2 levels, the concentration of HCO_3^- becomes important to the performance of the system due to its contribution to the total inorganic carbon pool. Since the bulk concentration of HCO_3^- is intrinsically linked to the concentration of CO_2 and pH, HCO_3^- levels are low in solutions purged with dilute CO_2 and are further depleted within the porous electrode when coupled to fast CO_2 hydration kinetics serving to offset local substrate consumption. In pH 7 MOPS, FEM shows that CA significantly reduces the HCO_3^- levels within the electrode at 1% CO_2 (0.59 vs 1.91 mM at −0.6 V vs SHE; bulk [HCO_3^-] = 1.96 mM) (Figure 4a). Since the predicted local HCO_3^- concentrations in 1% CO_2 experiments are much lower than the K_M of CA for HCO_3^- dehydration (8.3 mM), the consumption of HCO_3^- within the

electrode pores begins to limit CA's ability to replenish local CO_2 concentrations during electro-catalysis.[43]

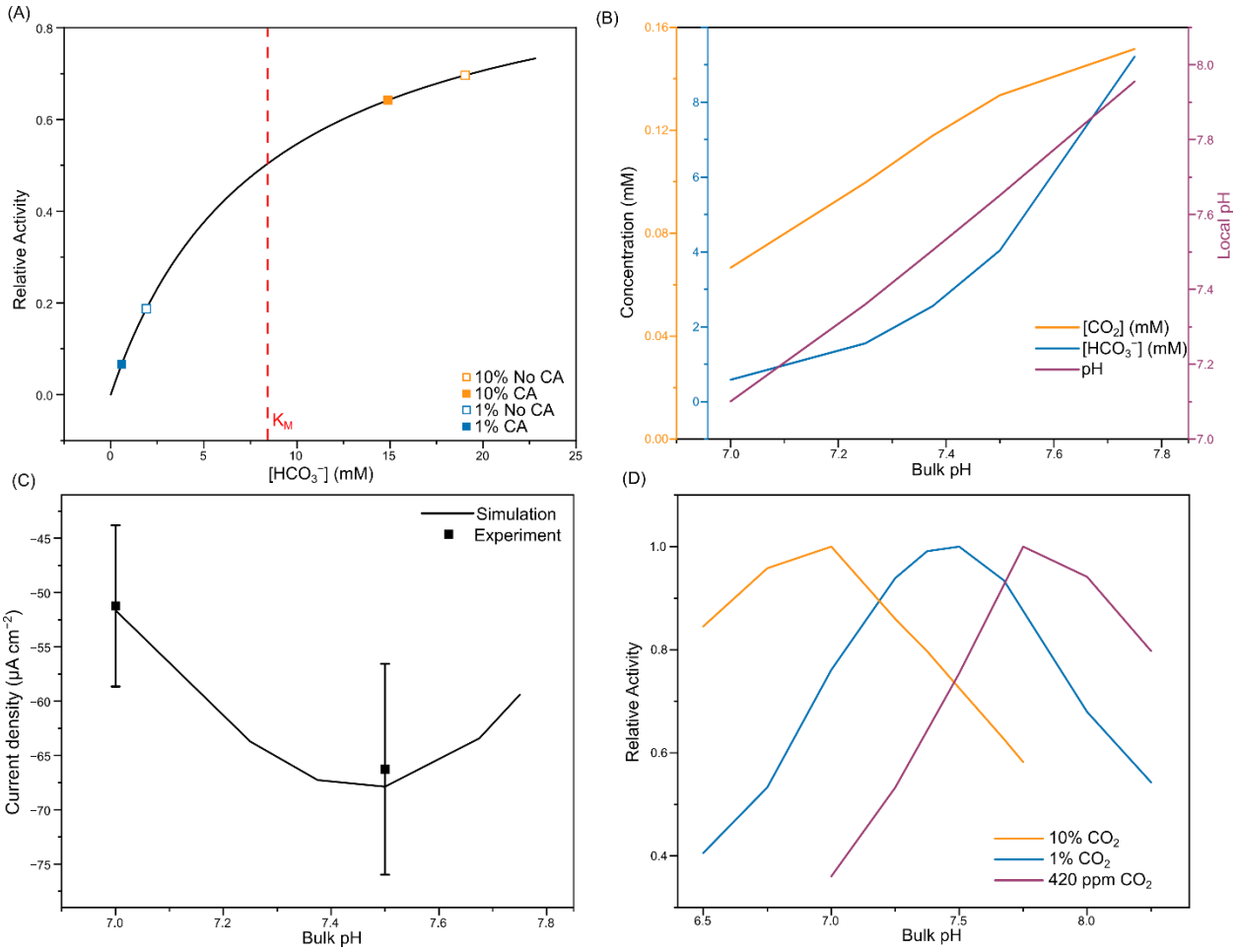

Figure 4. The effect of total dissolved carbon concentrations on the performance of a carboxysome mimic for low CO_2 (A). Local concentrations of HCO_3^- components at 10% (orange) and 1% (blue) bulk CO_2 concentrations obtained from FEM at −0.6 V vs SHE and its effect on CA activity ($K_{M,HCO3-}$= 8.3 mM). (B) Local pH (purple) and concentrations of CO_2 (orange) and HCO_3^- (blue) obtained from FEM at −0.6 V vs SHE for 1% CO_2 at a range of bulk pH with CA co-immobilization. (C) Experimental (points) and simulated (lines) current densities for CO_2R by FDh with CA co-immobilization at a range of bulk pH, showing an optimal at pH 7.5. (D) Effect of bulk pH on simulated relative activities for CO_2R by FDh with CA co-immobilization, showing a shift in the optimal pH as the bulk CO_2 concentration is reduced from 10% (orange) to 1% (blue) and 0.042% (atmospheric concentration, purple).

As the concentration of dissolved CO_2 is fixed by Henry's law and the [HCO_3^-] is dependent on the pH equilibrium between CO_2 and HCO_3^- in solution (pK_a: 6.28, Figure S7a), increasing the solution pH shifts the CO_2/HCO_3^- equilibrium by elevating dissolved HCO_3^- levels while keeping dissolved CO_2 concentrations relatively constant (Figure S7b). As a result, raising the solution pH increases the total dissolved carbon pool available for CO_2R ~10× per pH unit when paired with fast CO_2 hydration kinetics. This bulk increase gives higher local HCO_3^- concentrations as a result of increasing the solution pH (Figure 4b). The increased local carbon concentrations at higher bulk pH values act to increase activity, but the associated local pH increase is detrimental to enzymatic CO_2R (Fig. 3d).

To manage this tradeoff between local pH and local carbon concentration, the bulk pH determined from FEM to optimize CO_2R at 1% CO_2 increases to 7.5 (Figure 4c), a result confirmed experimentally. As CO_2 concentrations are reduced, the bulk pH that leads to the greatest improvement in enzymatic CO_2R with CA present can be shown by FEM to move to more basic values as the importance of increased substrate concentration outweighs the requirement to optimize the local pH for optimal activity (Figure 4d). This improvement in enzymatic CO_2R is contingent on the presence of CA as without fast CO_2 hydration kinetics, the increased local HCO_3^- concentrations cannot be used to elevate local substrate concentrations and the more basic bulk pH is merely detrimental to the activity of FDh.

Atmospheric concentration CO_2 reduction

When CO_2 concentrations are further reduced to the ultimate goal of atmospheric concentrations (420 ppm), optimization of the chemical environment within the porous electrode becomes vital to the performance of the carboxysome inspired system. FEM identified an optimal pH of 7.75 to offer a 2.8× improvement in fuel production over pH 7 (Figure 4d), with a reduced MOPS concentration of 25 mM to aid formate quantification. From the model, it was apparent that CA acts to greatly increase the current density for CO_2R at atmospheric CO_2 concentrations (7.8× at the optimal of pH 7.75 and 3.7× at pH 7), and that the bulk pH should be optimized to provide sufficient dissolved carbon without an overly basic pH that would reduce activity. At atmospheric concentrations, the concentration of CO_2 is below that of CA, as such the steady state assumptions of the Michaelis-Menten equation may no longer be valid, however modelling of natural carboxysomes have used unmodified Michaelis-Menten kinetics.[44,45] At atmospheric CO_2 concentrations, effective CO_2R at quantifiable rates becomes exceedingly challenging, and increased CO_2 hydration kinetics become crucial to its viability. To allow for quantification, FDh loading was increased to 100 pmol and experiments were performed for increased times (48 h) on TiO_2 electrodes (30 nm anatase, 12 ± 0.8 µm thickness, 0.196 cm^2, Figure S8) that give negligible background currents in constant potential electrolysis (Figure S9) at the expense of poor electrochemical performance at more positive potentials >−0.45 vs SHE.

While the experimental currents and charge densities were lower than simulated (Table S3), the trends were closely matched, demonstrating that while the model is approaching its useful limits for predicting the local environment and current densities it can still be highly beneficial for system design and optimization. Formate production after 48 h with CA was determined by IC quantification to be 0.22 ± 0.008 µmol cm^{-2} with a FE of 29 ± 7 at pH 7 and 0.69 ± 0.04 µmol cm^{-2} with a FE of 37 ± 4 at pH 7.75 at −0.6 V vs SHE. Product quantification was not possible without CA as the $HCOO^-$ was below the quantification limit (13 µM, corresponding to for-

mate production of 0.20 µmol cm^{-2} in a minimized solution volume of 3 mL, Figure S10), however was detectable in pH 7 with a concentration above the detection limit of 4.2 µM (64 nmol cm^{-2}) but below the quantification limit. This fits the expected trend from the model and highlights the benefit of this carboxysome inspired approach to manage the local environment. While the achieved current densities are low, these experiments demonstrate that CO_2R at atmospheric concentrations is greatly enhanced with higher dissolved HCO_3^- concentrations. This can be used to increase local CO_2 levels and current density when coupled to fast CO_2 hydration kinetics to remove the kinetic limitation that prevents HCO_3^- being utilized for enzymatic CO_2R at low CO_2 concentrations. This offers insights to the development of future catalyst systems as they approach the properties of enzymes, making the composition and availability of inorganic carbon in solution vital to their effective performance when integrated into real world systems.

Conclusions

The strategies employed by cyanobacteria to optimize carbon fixation can be used to develop effective systems for CO_2 utilization from low to atmospheric CO_2 concentrations. The co-immobilization of CA with FDh at concentrations comparable to the natural carboxysome allows the fast interconversion of HCO_3^- and CO_2, following the pH equilibrium. Without additional buffers, CA does not improve the CO_2R activity as its presence leads to a lower local pH that increases the FDh activity but is directly counteracted by the decrease in local CO_2 concentration that reduces the activity as the concentration drops below the K_m. Additional buffers such as MOPS are required to mitigate changes in local pH and prevent the increase in local pH that drives the HCO_3^-/CO_2 equilibrium towards HCO_3^-. CA improved the current density when MOPS was added to the solution, with a greater current density increase as the bulk CO_2 concentration decreased. This was due to an increased local CO_2 concentration, as HCO_3^- can act to replenish depleted CO_2 without large local pH changes. By raising the bulk pH, the amount of dissolved inorganic carbon is increased, leading to increases in CO_2R and demonstrating an ap-

proach that can be used to mimic the carboxysome for atmospheric concentration CO_2R. At atmospheric CO_2 concentrations, CA co-immobilization at an optimal pH of 7.75 allowed quantifiable formate production of 0.69 ± 0.04 μmol cm^{-2} for direct CO_2R without preconcentration at atmospheric concentrations. In this designed bioelectrochemical system, the co-immobilization of CA and FDh within mesoporous electrodes mimics the nanoconfinement of CA and RuBisCO within the carboxysome's protein shell, and the alkaline pH mimics the cyanobacterial cytosol. Together these interventions greatly enhance CO_2R at low CO_2 concentrations minimizing substrate depletion at the electrode. This carboxysome inspired strategy for the direct reduction of CO_2 at atmospheric concentrations may advance the long-standing goal of atmospheric CO_2R by elevating substrate concentrations that can limit fuel production from low-concentration sources.

Acknowledgments

This work was supported by a European Research Council (ERC) Consolidator Grant (MatEnSAP, no. 682833; S.J.C, E.R.), the Leverhulme Trust for a research project grant (P80336; to S.J.C, E.R.) and Early Career Fellowship (ECF-2021-072, S.J.C), the Isaac Newton Trust(20.08(r),S.J.C.) the Winston Churchilll Foundation of the United States (A.D.), the Fundação para a Ciência e Tecnologia (FCT, Portugal) for fellowship SFRH/BD/116515/2016 (A.R.O.), grant PTDC/BII-BBF/2050/2020 (I.A.C.P.) and MOSTMICRO-ITQB unit (UIDB/04612/2020 and UIDP/04612/2020), and EU Horizon 2020 R&I programme 810856. We thank Vivek Badiani for useful discussions.

Data and materials availability

All data are available in the main text or the supplementary materials or available on the Cambridge Apollo repository upon publication.

References

(1) Artz, J.; Müller, T. E.; Thenert, K.; Kleinekorte, J.; Meys, R.; Sternberg, A.; Bardow, A.; Leitner, W. Sustainable Conversion of Carbon Dioxide: An Integrated Review of Catalysis and Life Cycle Assessment. *Chem. Rev.* **2018**, *118*, 434–504.

(2) Kumagai, H.; Nishikawa, T.; Koizumi, H.; Yatsu, T.; Sahara, G.; Yamazaki, Y.; Tamaki, Y.; Ishitani, O. Electrocatalytic Reduction of Low Concentration CO_2. *Chem. Sci.* **2019**, *10*, 1597–1606.

(3) Nakajima, T.; Tamaki, Y.; Ueno, K.; Kato, E.; Nishikawa, T.; Ohkubo, K.; Yamazaki, Y.; Morimoto, T.; Ishitani, O. Photocatalytic Reduction of Low Concentration of CO_2. *J. Am. Chem. Soc.* **2016**, *138*, 13818–13821.

(4) Keith, D. W.; Holmes, G.; St. Angelo, D.; Heidel, K. A Process for Capturing CO_2 from the Atmosphere. *Joule* **2018**, *2*, 1573–1594.

(5) Koytsoumpa, E. I.; Bergins, C.; Kakaras, E. The CO_2 Economy: Review of CO_2 Capture and Reuse Technologies. *J. Supercrit. Fluids* **2018**, *132*, 3–16.

(6) Sharifian, R.; Wagterveld, R. M.; Digdaya, I. A.; Xiang, C.; Vermaas, D. A. Electrochemical Carbon Dioxide Capture to Close the Carbon Cycle. *Energy Environ. Sci.* **2021**, *14*, 781–814.

(7) Xie, H.; Jiang, W.; Liu, T.; Wu, Y.; Wang, Y.; Chen, B.; Niu, D.; Liang, B. Low-Energy Electrochemical Carbon Dioxide Capture Based on a Biological Redox Proton Carrier. *Cell Reports Phys. Sci.* **2020**, *1*, 100046.

(8) D'Alessandro, D. M.; Smit, B.; Long, J. R. Carbon Dioxide Capture: Prospects for New Materials. *Angew. Chemie - Int. Ed.* **2010**, *49*, 6058–6082.

(9) Xu, Y.; Edwards, J. P.; Zhong, J.; O'Brien, C. P.; Gabardo, C. M.; McCallum, C.; Li, J.; Dinh, C. T.; Sargent, E. H.; Sinton, D. Oxygen-Tolerant Electroproduction of C2 Products

from Simulated Flue Gas. *Energy Environ. Sci.* **2020**, *13*, 554–561.

(10) Shively, J. M.; Ball, F.; Brown, D. H.; Saunders, R. E. Functional Organelles in Prokaryotes: Polyhedral Inclusions (Carboxysomes) of Thiobacillus Neapolitanus. *Science (80-.).* **1973**, *182*, 584–586.

(11) Yeates, T. O.; Kerfeld, C. A.; Heinhorst, S.; Cannon, G. C.; Shively, J. M. Protein-Based Organelles in Bacteria: Carboxysomes and Related Microcompartments. *Nat. Rev. Microbiol.* **2008**, *6*, 681–691.

(12) Maccready, J. S.; Vecchiarelli, A. G. Positioning the Model Bacterial Organelle, the Carboxysome. *MBio* **2021**, *12*.

(13) Lan, Y.; Mott, K. A. Determination of Apparent Km Values for Ribulose 1,5-Bisphosphate Carboxylase/Oxygenase (Rubisco) Activase Using the Spectrophotometric Assay of Rubisco Activity. *Plant Physiol.* **1991**, *95*, 604–609.

(14) Bowes, G.; Ogren, W. L. Oxygen Inhibition and Other Properties of Soybean Ribulose 1,5-Diphosphate Carboxylase. *J. Biol. Chem.* **1972**, *247*, 2171–2176.

(15) Khalifah, R. G. The Carbon Dioxide Hydration Activity of Carbonic Anhydrase. *J. Biol. Chem.* **1971**, *246*, 2561–2573.

(16) Price, G. D.; Woodger, F. J.; Badger, M. R.; Howitt, S. M.; Tucker, L. Identification of a SulP-Type Bicarbonate Transporter in Marine Cyanobacteria. *Proc. Natl. Acad. Sci. U. S. A.* **2004**, *101*, 18228–18233.

(17) Price, G. D.; Badger, M. R.; Woodger, F. J.; Long, B. M. Advances in Understanding the Cyanobacterial CO_2 -Concentrating- Mechanism (CCM): Functional Components, Ci Transporters, Diversity, Genetic Regulation and Prospects for Engineering into Plants. *J. Exp. Bot.* **2008**, *59*, 1441–1461.

(18) Welch, A. J.; Dunn, E.; Duchene, J. S.; Atwater, H. A. Bicarbonate or Carbonate Processes for Coupling Carbon Dioxide Capture and Electrochemical Conversion. *ACS Energy Letters*. 2020, pp 940–945.

(19) Deng, W.; Yuan, T.; Chen, S.; Li, H.; Hu, C.; Dong, H.; Wu, B.; Wang, T.; Li, J.; Ozin, G. A.; Gong, J. Effect of Bicarbonate on CO_2 Electroreduction over Cathode Catalysts. *Fundam. Res.* **2021**, *1*, 432–438.

(20) Li, T.; Lees, E. W.; Goldman, M.; Salvatore, D. A.; Weekes, D. M.; Berlinguette, C. P. Electrolytic Conversion of Bicarbonate into CO in a Flow Cell. *Joule* **2019**, *3*, 1487–1497.

(21) Lees, E. W.; Goldman, M.; Fink, A. G.; Dvorak, D. J.; Salvatore, D. A.; Zhang, Z.; Loo, N. W. X.; Berlinguette, C. P. Electrodes Designed for Converting Bicarbonate into CO. *ACS Energy Lett.* **2020**, *5*, 2165–2173.

(22) Lees, E. W.; Bui, J. C.; Song, D.; Weber, A. Z.; Berlinguette, C. P. Continuum Model to Define the Chemistry and Mass Transfer in a Bicarbonate Electrolyzer. *ACS Energy Lett.* **2022**, *7*, 834–842.

(23) Li, Y. C.; Lee, G.; Yuan, T.; Wang, Y.; Nam, D. H.; Wang, Z.; Garciá De Arquer, F. P.; Lum, Y.; Dinh, C. T.; Voznyy, O.; Sargent, E. H. CO_2 Electroreduction from Carbonate Electrolyte. *ACS Energy Lett.* **2019**, *4*, 1427–1431.

(24) Lee, G.; Li, Y. C.; Kim, J. Y.; Peng, T.; Nam, D. H.; Sedighian Rasouli, A.; Li, F.; Luo, M.; Ip, A. H.; Joo, Y. C.; Sargent, E. H. Electrochemical Upgrade of CO_2 from Amine Capture Solution. *Nat. Energy* **2021**, *6*, 46–53.

(25) Chen, L.; Li, F.; Zhang, Y.; Bentley, C. L.; Horne, M.; Bond, A. M.; Zhang, J. Electrochemical Reduction of Carbon Dioxide in a Monoethanolamine Capture Medium. *ChemSusChem* **2017**, *10*, 4109–4118.

(26) Kar, S.; Goeppert, A.; Prakash, G. K. S. Integrated CO_2 Capture and Conversion to Formate and Methanol: Connecting Two Threads. *Acc. Chem. Res.* **2019**, *52*, 2892–2903.

(27) Meneghello, M.; Oliveira, A. R.; Jacq-Bailly, A.; Pereira, I. A. C.; Léger, C.; Fourmond, V. Formate Dehydrogenases Reduce CO_2 Rather than HCO_3^-: An Electrochemical Demonstration. *Angew. Chemie - Int. Ed.* **2021**, *60*, 1–5.

(28) Cobb, S. J.; Badiani, V. M.; Dharani, A. M.; Wagner, A.; Zacarias, S.; Oliveira, A. R.; Pereira, I. A. C.; Reisner, E. Fast CO_2 Hydration Kinetics Impair Heterogeneous, but Improve Enzymatic CO_2 Reduction Catalysis. *Nat. Chem.* **2022**, *4*, 417–424.

(29) Addo, P. K.; Arechederra, R. L.; Waheed, A.; Shoemaker, J. D.; Sly, W. S.; Minteer, S. D. Methanol Production via Bioelectrocatalytic Reduction of Carbon Dioxide: Role of Carbonic Anhydrase in Improving Electrode Performance. *Electrochem. Solid-State Lett.* **2011**, *14*, 5–10.

(30) Sato, R.; Amao, Y. Carbonic Anhydrase/Formate Dehydrogenase Bienzymatic System for CO_2 Capture, Utilization and Storage. *React. Chem. Eng.* **2022**, *7*, 181–191.

(31) Srikanth, S.; Alvarez-Gallego, Y.; Vanbroekhoven, K.; Pant, D. Enzymatic Electrosynthesis of Formic Acid through Carbon Dioxide Reduction in a Bioelectrochemical System: Effect of Immobilization and Carbonic Anhydrase Addition. *ChemPhysChem* **2017**, *18*, 3174–3181.

(32) Vannoy, K. J.; Lee, I.; Sode, K.; Dick, J. E. Electrochemical Quantification of Accelerated FADGDH Rates in Aqueous Nanodroplets. *Proc. Natl. Acad. Sci. U. S. A.* **2021**, *118*, e2025726118.

(33) Shekh, A. Y.; Krishnamurthi, K.; Mudliar, S. N.; Yadav, R. R.; Fulke, A. B.; Devi, S. S.; Chakrabarti, T. Recent Advancements in Carbonic Anhydrase-Driven Processes for CO_2 Sequestration: Minireview. *Crit. Rev. Environ. Sci. Technol.* **2012**, *42*, 1419–1440.

(34) Fink, A. G.; Lees, E. W.; Gingras, J.; Madore, E.; Fradette, S.; Jaffer, S. A.; Goldman, M.; Dvorak, D. J.; Berlinguette, C. P. Electrolytic Conversion of Carbon Capture Solutions Containing Carbonic Anhydrase. *J. Inorg. Biochem.* **2022**, *231*, 111782.

(35) Sullivan, I.; Goryachev, A.; Digdaya, I. A.; Li, X.; Atwater, H. A.; Vermaas, D. A.; Xiang, C. Coupling Electrochemical CO_2 Conversion with CO_2 Capture. *Nat. Catal.* **2021**, *4*, 952–958.

(36) Zhang, S.; Chen, C.; Li, K.; Yu, H.; Li, F. Materials and System Design for Direct

Electrochemical CO_2 Conversion in Capture Media. *J. Mater. Chem. A* **2021**, *9*, 18785–18792.

(37) Oliveira, A. R.; Mota, C.; Mourato, C. C. C.; Domingos, R. M.; Santos, M. F. A.; Gesto, D.; Guigliarelli, B.; Santos-Silva, T.; Romão, M. J.; Cardoso Pereira, I. A.; Romaõ, M. J.; Cardoso Pereira, I. A. Toward the Mechanistic Understanding of Enzymatic CO_2 Reduction. *ACS Catal.* **2020**, *10*, 3844–3856.

(38) Moore, E. E.; Cobb, S. J.; Coito, A. M.; Oliveira, A. R.; Pereira, I. A. C.; Reisner, E.; Edwardes Moore, E.; Cobb, S. J.; Coito, A. M.; Oliveira, A. R.; Pereira, I. A. C.; Reisner, E. Understanding the Local Chemical Environment of Bioelectrocatalysis. *Proc. Natl. Acad. Sci. U. S. A.* **2022**, *119*, e2114097119.

(39) Liu, L.; Yellinek, S.; Valdinger, I.; Donval, A.; Mandler, D. Important Implications of the Electrochemical Reduction of ITO. *Electrochim. Acta* **2015**, *176*, 1374–1381.

(40) Ciocci, P.; Lemineur, J. F.; Noël, J. M.; Combellas, C.; Kanoufi, F. Differentiating Electrochemically Active Regions of Indium Tin Oxide Electrodes for Hydrogen Evolution and Reductive Decomposition Reactions. An in Situ Optical Microscopy Approach. *Electrochim. Acta* **2021**, *386*, 138498.

(41) Geiger, S.; Kasian, O.; Mingers, A. M.; Mayrhofer, K. J. J.; Cherevko, S. Stability Limits of Tin-Based Electrocatalyst Supports. *Sci. Rep.* **2017**, *7*, 3–9.

(42) Monteiro, M. C. O.; Koper, M. T. M. Measuring Local PH in Electrochemistry. *Curr. Opin. Electrochem.* **2021**, *25*, 100649.

(43) Lindskog, S.; Coleman, J. E. The Catalytic Mechanism of Carbonic Anhydrase. *Proc. Natl. Acad. Sci. U. S. A.* **1973**, *70*, 2505–2508.

(44) Mangan, N. M.; Flamholz, A.; Hood, R. D.; Milo, R.; Savage, D. F. PH Determines the Energetic Efficiency of the Cyanobacterial CO_2 Concentrating Mechanism. *Proc. Natl. Acad. Sci. U. S. A.* **2016**, *113*, E5354–E5362.

(45) Long, B. M.; Förster, B.; Pulsford, S. B.; Price, G. D.; Badger, M. R. Rubisco Proton

Production Can Drive the Elevation of CO_2 within Condensates and Carboxysomes. *Proc. Natl. Acad. Sci. U. S. A.* **2021**, *118*.

TOC graphic

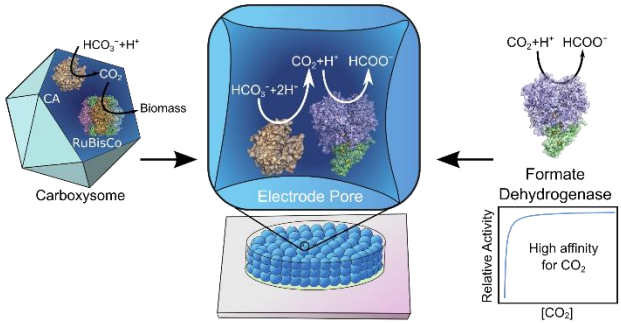
$HCO_3^-+H^+$
CO_2
CA
Biomass
RuBisCo
Carboxysome
CO_2+H^+ $HCOO^-$
$HCO_3^-+2H^+$
Electrode Pore
CO_2+H^+ $HCOO^-$
Formate
Dehydrogenase
Relative Activity
High affinity
for CO_2
$[CO_2]$